Quantitative Atomic Resolution Scanning Transmission Electron Microscopy

James M. LeBeau,[1,*] Scott D. Findlay,[2] Leslie J. Allen,[3] and Susanne Stemmer[4,†]

[1]*Materials Department, University of California, Santa Barbara, California 93106-5050, USA*
[2]*Institute of Engineering Innovation, School of Engineering, The University of Tokyo, Tokyo, 113-8656, Japan*
[3]*School of Physics, University of Melbourne, Victoria 3010, Australia*
[4]*Materials Department, University of California, Santa Barbara, California 93106-5050, USA*

(Received 1 February 2008; revised manuscript received 16 April 2008; published 23 May 2008)

Complete understanding of atomic resolution high-angle annular dark-field (*Z*-contrast) images requires quantitative agreement between simulations and experiments. We show that intensity variations can be placed on an absolute scale by normalizing the measured image intensities to the incident beam. We construct fractional intensity images of a $SrTiO_3$ single crystal for regions of different thickness up to 120 nm. Experimental images are compared directly with image simulations. Provided that spatial incoherence is taken into account in the simulations, almost perfect agreement is found between simulation and experiment.

DOI: 10.1103/PhysRevLett.100.206101 PACS numbers: 68.37.Lp

High-angle annular dark-field (HAADF) or *Z*-contrast imaging in scanning transmission electron microscopy (STEM) provides atomic structure images with excellent atomic-number (*Z*) sensitivity [1] and has been applied to determine the precise location and identity of individual atoms and clusters [2,3], with sub-Ångstrom resolution [4] and in three dimensions [5,6]. While qualitative interpretation often gives a general indication of the structure, image simulations are required to make the technique truly quantitative, in particular, for the analysis of defects. Where attempts have been made to achieve quantitative *Z*-contrast imaging, lower contrast in the experiments has been noted [7,8]. This is not unlike the situation in conventional high-resolution transmission electron microscopy (HRTEM), which uses an incident plane wave rather than a focused probe [9]. The origin of this mismatch, known as the "Stobbs' factor" [10], has not yet been identified [10–15]. Scientifically, these discrepancies raise the crucial question as to whether current simulations of image contrast formation are inadequate, perhaps neglecting significant contributions to the scattering of high-energy electrons by crystalline materials. For example, existing HAADF imaging theories include thermal diffuse (phonon) scattering [16,17]. It is conceivable that more sophisticated phonon models [18] or inclusion of other inelastic scattering processes [11,19] may be required.

Simulations provide the image intensity variation on a scale that is normalized to the incident beam intensity. To date, quantitative comparisons with experiments have all required scaling the experimental intensity values to the simulations since the experimental data were not determined on an absolute scale [7,8,20,21]. Such comparisons limit the ability to completely understand the physics of HAADF image contrast [10]. For example, the lower contrast in experiments can be interpreted as being due to an underestimation of the minimum intensity in the simulated images ("background signal"), which in HAADF constitutes a substantial fraction (tens of percent for typical thicknesses) of the maximum image intensity [7]. An alternative explanation is that simulations are overestimating the signal at the atomic columns [8]. These two possibilities cannot be distinguished without a measure of the fraction of incident electrons contributing to the HAADF signal.

In this Letter, we show that measurement of the incident beam intensity and the HAADF signal is possible using an annular dark-field detector that has single electron sensitivity and an output voltage that is directly proportional to the electron flux averaged over time (intensity). This HAADF detector greatly facilitates quantitative measurements. In contrast, charge-couple device (CCD) cameras are often employed in HRTEM, requiring corrections for noise and the CCD response function [22]. Here, truly quantitative, atomically resolved *Z*-contrast images normalized to the incident beam intensity are obtained for a $SrTiO_3$ single crystal. Image simulations of normalized intensities show excellent agreement after accounting for spatial incoherence.

TEM samples were prepared by wedge polishing followed by Ar-ion milling and buffered HF etching to remove amorphous surface layers. Image and incident probe intensities were measured with a field-emission transmission electron microscope (FEI Titan 80–300 TEM/STEM) with a supertwin lens ($C_s = 1.2$ mm) operated at 300 kV and equipped with an annular dark-field detector (Fischione Model 3000). The convergence semiangle was 9.6 ± 0.15 mrad and the inner detector semiangle was 65 ± 1 mrad. The focus (54 nm underfocus) was determined using the maximum intensity criterion in both experiments and simulations, as described previously [7,8]. A Gatan Enfina spectrometer with a collection aperture of 15 ± 0.3 mrad was used for electron energy-loss spectroscopy (EELS).

The HAADF signal and incident probe (entire beam on the detector) was measured by connecting a National Instruments dynamic signal analyzer (model number

4474) to the detector preamplifier. Linearity of the detector and preamplifier response for the chosen gain and offset settings was confirmed by measuring the output voltage as a function of the Schottky emitter extraction voltage and verifying that the signal followed the known relationship between extraction voltage and intensity [23]. Only a relatively low intensity probe could be used without saturating the detector preamplifier. The acquisition time for the 1024×1024 images was 61.68 s. The time that the probe spends at each pixel (dwell time) determines how many voltage measurements are associated with each pixel in the final image. The detector output was oversampled by roughly a factor of 5. Image pixel values were obtained by down-sampling and normalizing the signal to the incident probe intensity. No further image processing was performed. From these images, average values for the normalized intensities of the Sr and Ti-O atom columns and that of the background were determined. The reported intensities of the signal with the probe on an atomic column are averages of the centroid intensity value of each column in the entire image. The centroids were found by standard image processing procedures, including thresholding to find the column boundaries [24]. The intensities at the full-width at half-maxima (FWHMs) of the Ti-O and Sr columns were sufficiently different so that the areas within the column boundaries could be used to identify the column type. The error bars represent standard deviations from the mean intensity values in one image (400–600 columns per image). The background intensity, when the probe is located between the columns, was taken as the average of the lowest 2% of all image pixel values. The use of a finite range (up to 2%) was required because of the noise in the background intensities (caused by the detector noise level). Bloch wave HAADF image simulations were carried out using the mixed dynamical form factor approach for thermal diffuse scattering (phonon excitation) [17] as were multislice frozen phonon model calculations [25]. Debye-Waller factors were taken from the literature [26]. The outer detector semiangle for the calculations was 240 mrad [27]. The frozen phonon simulations were carried out with a limited number of sampling points and phonon passes (for details see Ref. [8]) to achieve realistic computing times for thick samples.

Figure 1 (top row) shows experimental HAADF images of a $SrTiO_3$ single crystal recorded along $\langle 100 \rangle$ for regions with three different thicknesses (25, 55, and 105 nm). Image intensities are represented in terms of fractions of the incident beam signal (see color scale bar on the right). For the largest thickness, 21% of the incident beam intensity is scattered thermally to contribute to the signal when the probe is on the atomic columns compared with 12% when the probe is located between columns.

Having normalized the image intensity, the remaining experimental challenge is determining the TEM foil thickness t. In EELS, ratios of $\ln(I_t/I_0)$ are sensitive to thickness changes (I_t is the total area under the spectrum, I_0 the area under the zero-loss peak) and determine t/λ, where λ is the total bulk inelastic mean free path [28]. The bulk plasmon

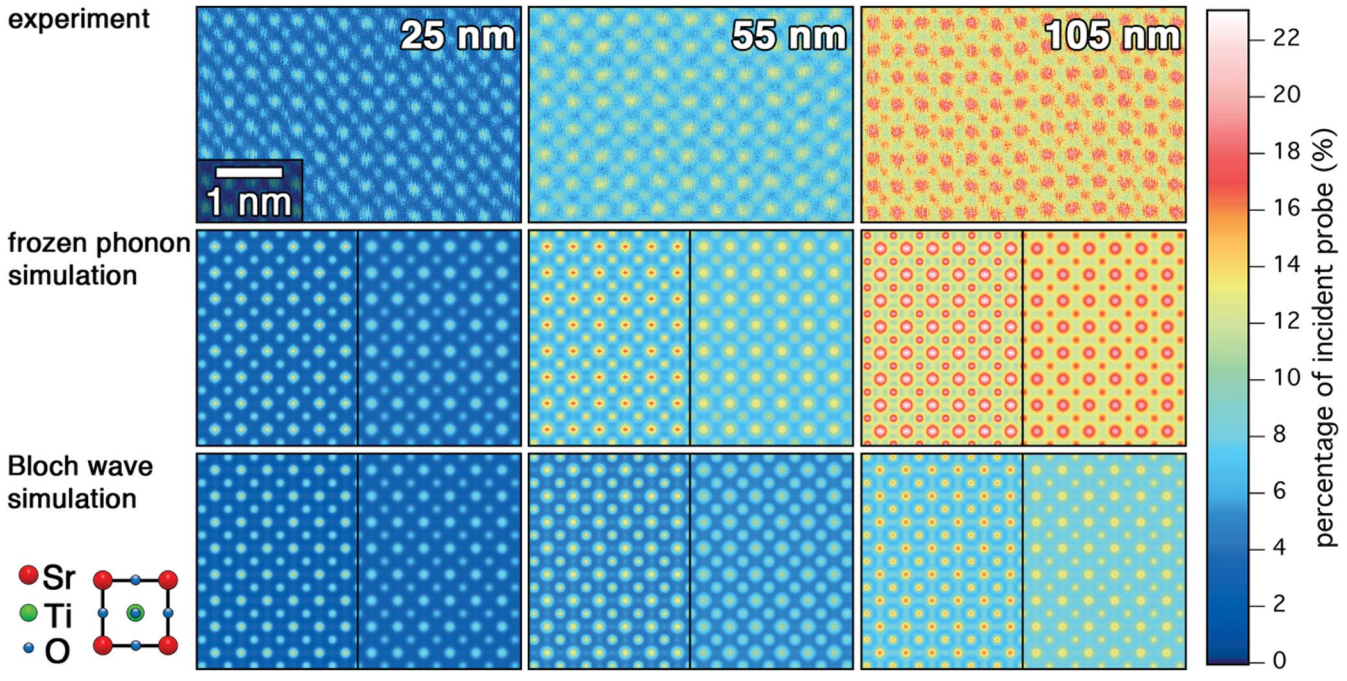

FIG. 1 (color). Top row: experimental HAADF images of $SrTiO_3$ along $\langle 100 \rangle$ with intensity variations normalized to the incident beam intensity (see color scale bar on the right). Regions of three different thicknesses are shown. The Sr columns are the brightest and the Ti-O columns are the second brightest features (see unit cell schematic on the left). The image of the 105 nm region has been drift corrected. Middle row: frozen phonon image simulations. Bottom row: Bloch wave image simulations. In each case, simulations are shown without (left pane) and with convolution with a 0.08 nm FWHM Gaussian (right pane).

scattering inelastic mean free path λ_B can be estimated (123 nm for $SrTiO_3$) [28]. To a first approximation, surface plasmon losses result in an offset to the thickness values obtained from $t = \lambda_B \ln(I_t/I_0)$ [29]. This correction, Δt_S, was estimated from the linear thickness dependence of the background signal in HAADF, which must extrapolate to zero at zero thickness. For $SrTiO_3$, the required correction Δt_S was -29 nm. The pronounced surface plasmon feature (Fig. 2, dashed line) in a region with $t < 5$ nm [yielding $\ln(I_t/I_0) = 0.27$ in this region] suggests that strong surface contributions are important in $SrTiO_3$.

Figure 1 also shows image simulations using frozen phonon and Bloch wave calculations (middle and bottom rows). Those shown in the left pane in each case do not take spatial incoherence into account. While a qualitative match exists between simulations and experiments, there are quantitative differences; in particular, the contrast is higher in the simulations. Spatial incoherence (defined here as combined effects from a finite extent of the effective illumination source, instabilities, sample drift, etc.) is known to reduce the contrast and can be modeled by convolving the simulated HAADF images by a Gaussian envelope function [8,30]. A Gaussian with a FWHM of 0.08 nm (right pane) provided excellent agreement with the experimental data. For thick regions, the discrepancies between the signal strength in Bloch wave simulations and experiments evident in Fig. 1 are expected, because this approach does not include further elastic or inelastic scattering after thermal scattering events [8]. For thicknesses greater than 40 nm these events become important, requiring the use of the frozen phonon approach [8,25]. The quantitative agreement between the two simulation approaches for thin regions showed that it is tolerable to use a small number of phonon configurations and probe positions in the frozen phonon calculations.

Figure 3 compares the experimental fractional intensities with the probe situated between the columns (I_B), on the Sr columns (I_{Sr}) and on the Ti-O ($I_{Ti\text{-}O}$) columns, and the corresponding values from the frozen phonon and Bloch wave simulations. Without taking spatial incoherence into account [Fig. 3(a)] the column intensities in the simulations were considerably greater than in the experiments. However, the background signal in experiments and simulations was very similar. This result tells strongly against the interpretation that the contrast problem in $SrTiO_3$ is due to simulations underestimating the background; thermal scattering alone is sufficient to quantitatively predict the measured background, without any recourse to additional inelastic scattering mechanisms. Taking into account spatial incoherence, via a Gaussian envelope of 0.08 nm FWHM [Fig. 3(b)], leads to almost perfect agreement between simulation and experiment on

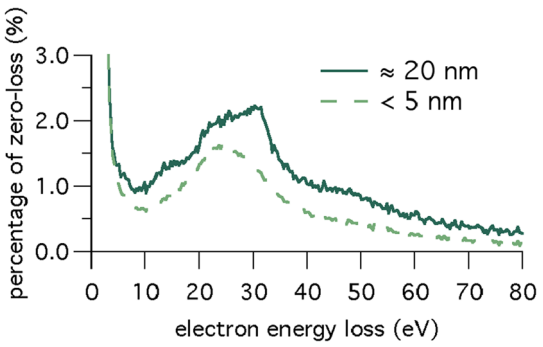

FIG. 2 (color online). Low loss EELS from one of the thinnest (<5 nm) crystalline areas (dashed line) and from a 20 nm thick area (solid line). Note the strong surface plasmon feature at 24.3 eV in the thin region. The energy of the surface plasmon is similar to what has been reported in the literature (see Ref. [32]). The thicker region shows interband transition, bulk, and surface plasmon losses.

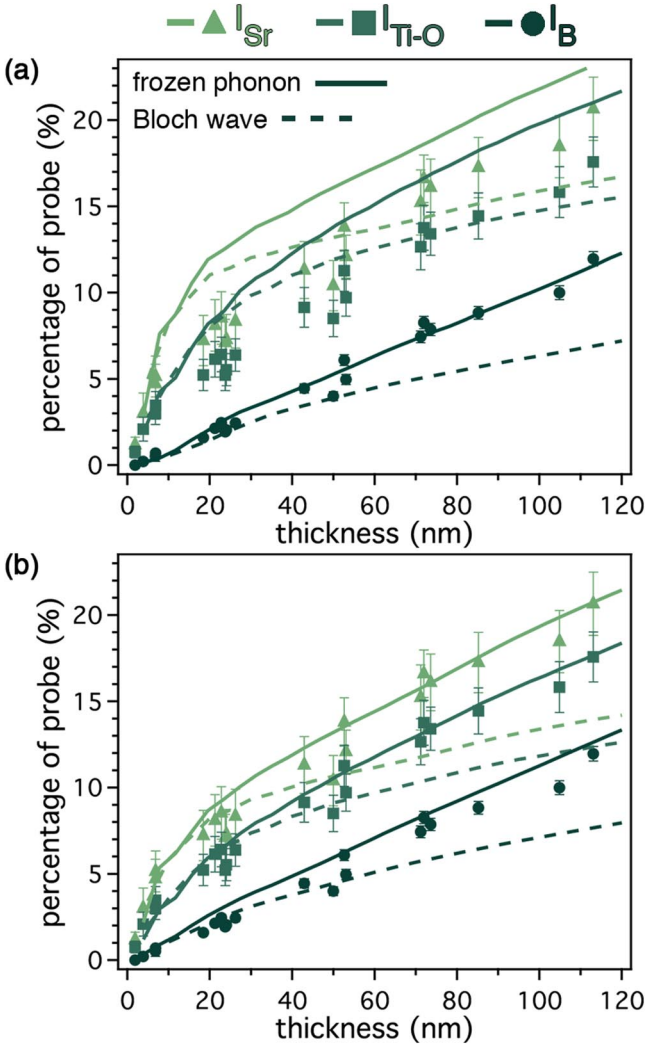

FIG. 3 (color online). (a) Experimental (symbols) and simulated (lines) Sr and Ti-O column and background intensity values for $SrTiO_3$ along ⟨100⟩ in terms of fraction of the incident beam intensity as a function of thickness. (b) Same as in (a) but with a 0.08 nm FWHM envelope modeling spatial incoherence in the simulations. The error bars reflect the standard deviations calculated from 400–600 columns for each thickness.

the atomic columns at small thicknesses for the Bloch wave approach and the whole thickness range for the frozen phonon model.

A finite source size described by a 0.08 nm FWHM Gaussian is a reasonable estimate of the spatial incoherence for this microscope because a similar spherical aberration (probe) corrected microscope was shown to have an information limit (determined by spatial incoherence) in HAADF of 0.08 nm [31]. Thus we anticipate that comparisons between simulations and experiments using aberration corrected instruments will require similar corrections for spatial incoherence. Detector preamplifiers with a wider dynamic range will, however, be needed for measurements of the intense incident probes used in aberration corrected STEM.

In summary, we have shown that image intensities in Z-contrast imaging can be placed on an absolute scale. These experiments allow for truly quantitative comparisons with theory and we recommend that all future HAADF experiments report normalized image intensities. We have demonstrated excellent agreement between image simulations and experiments, after taking into account spatial incoherence. Moreover, thermal scattering alone was sufficient to quantitatively predict the measured background. The agreement between theory and experiment is far better than for conventional HRTEM, where a large mismatch (a factor of around 2 to 3) is usual [9,13,15]. Quantitative HAADF demonstrates that existing models of thermal diffuse scattering provide for a quantitative description of the high-angle thermal diffuse scattering of high-energy electrons in $SrTiO_3$. Multiple thermal scattering, easily incorporated in the frozen phonon model, becomes important for thicker specimens. We have also shown that the background intensity in HAADF images, in conjunction with EELS, facilitates thickness estimates, in particular, in the presence of strong surface plasmons. Future experiments should explore the agreement between simulations and experiments for samples containing higher atomic numbers.

S. S. and J. M. L. acknowledge the U.S. DOE for support of this research (No. DE-FG02-06ER45994). J. M. L. also thanks the U.S. Department of Education (GAANN program No. P200A07044). L. J. A. acknowledges support by the Australian Research Council. S. D. F. is supported by the Japan Society for Promotion of Science (JSPS). We thank Mr. Zahid Chishty and Dr. Fred Kiewiet of FEI for discussions. This work made use of the UCSB MRL Central facilities (NSF No. DMR 05-20415).

*lebeau@mrl.ucsb.edu
†stemmer@mrl.ucsb.edu

[1] S. J. Pennycook and L. A. Boatner, Nature (London) **336**, 565 (1988).
[2] P. M. Voyles, D. A. Muller, J. L. Grazul, P. H. Citrin, and H. J. L. Gossmann, Nature (London) **416**, 826 (2002).
[3] A. Singhal, J. C. Yang, and J. M. Gibson, Ultramicroscopy **67**, 191 (1997).
[4] P. D. Nellist, M. F. Chisholm, N. Dellby, O. L. Krivanek, M. F. Murfitt, Z. S. Szilagyi, A. R. Lupini, A. Borisevich, W. H. Sides, and S. J. Pennycook, Science **305**, 1741 (2004).
[5] I. Arslan, T. J. V. Yates, N. D. Browning, and P. A. Midgley, Science **309**, 2195 (2005).
[6] A. Y. Borisevich, A. R. Lupini, and S. J. Pennycook, Proc. Natl. Acad. Sci. U.S.A. **103**, 3044 (2006).
[7] D. O. Klenov and S. Stemmer, Ultramicroscopy **106**, 889 (2006).
[8] D. O. Klenov, S. D. Findlay, L. J. Allen, and S. Stemmer, Phys. Rev. B **76**, 014111 (2007).
[9] M. J. Hÿtch and W. M. Stobbs, Ultramicroscopy **53**, 191 (1994).
[10] A. Howie, Ultramicroscopy **98**, 73 (2004).
[11] K. A. Mkhoyan, S. E. Maccagnano-Zacher, M. G. Thomas, and J. Silcox, Phys. Rev. Lett. **100**, 025503 (2008).
[12] H. Lichte, Phil. Trans. R. Soc. A **360**, 897 (2002).
[13] C. B. Boothroyd, J. Microsc. **190**, 99 (1998).
[14] C. B. Boothroyd and R. E. Dunin-Borkowski, Ultramicroscopy **98**, 115 (2004).
[15] K. Du, K. v. Hochmeister, and F. Phillipp, Ultramicroscopy **107**, 281 (2007).
[16] R. F. Loane, P. Xu, and J. Silcox, Ultramicroscopy **40**, 121 (1992).
[17] L. J. Allen, S. D. Findlay, M. P. Oxley, and C. J. Rossouw, Ultramicroscopy **96**, 47 (2003).
[18] D. A. Muller, B. Edwards, E. J. Kirkland, and J. Silcox, Ultramicroscopy **86**, 371 (2001).
[19] A. L. Bleloch, M. R. Castell, A. Howie, and C. A. Walsh, Ultramicroscopy **54**, 107 (1994).
[20] S. C. Anderson, C. R. Birkeland, G. R. Anstis, and D. J. H. Cockayne, Ultramicroscopy **69**, 83 (1997).
[21] J. Jiang, J. Yuan, and A. Bleloch, Appl. Phys. Lett. **91**, 113107 (2007).
[22] R. R. Meyer and A. I. Kirkland, Microsc. Res. Tech. **49**, 269 (2000).
[23] L. W. Swanson and G. A. Schwind, in *Handbook of Charged Particle Optics*, edited by J. Orloff (CRC Press LLC, Boca Raton, 1997).
[24] R. C. Gonzalez and R. E. Woods, *Digital Image Processing* (Prentice Hall, Englewood Cliffs, NJ, 2007), 3rd ed.
[25] R. F. Loane, P. R. Xu, and J. Silcox, Acta Crystallogr. Sect. A **47**, 267 (1991).
[26] Y. P. Peng, P. D. Nellist, and S. J. Pennycook, J. Electron Microsc. **53**, 257 (2004).
[27] This is smaller than the experimental value. Increasing the outer angle in the calculations to 400 mrad (the approximate detector range) did not significantly affect the contrast.
[28] R. F. Egerton, *Electron Energy-Loss Spectroscopy in the Electron Microscope* (Plenum Press, New York, 1996), 2nd ed.
[29] R. F. Egerton and S. C. Cheng, Ultramicroscopy **21**, 231 (1987).
[30] P. D. Nellist and J. M. Rodenburg, Ultramicroscopy **54**, 61 (1994).
[31] M. van d. Stam, M. Stekelenburg, B. Freitag, D. Herbert, and J. Rignalda, Microsc. Anal. **19**, 9 (2005).
[32] M. Kamaratos, D. Vlachos, and S. D. Foulias, Surf. Rev. Lett. **12**, 721 (2005).